



## A neutral dinuclear Ir(III) complex for anti-counterfeiting and data encryption

Received 00th January 20xx,  
Accepted 00th January 20xx

Yang Jiang,<sup>a</sup> Guangfu Li,<sup>a</sup> Weilong Che,<sup>a</sup> Yingjie Liu,<sup>b</sup> Bin Xu,<sup>b</sup> Guogang Shan,<sup>a</sup> Dongxia Zhu,<sup>\*a</sup>  
Zhongmin Su,<sup>\*a</sup> Martin R. Bryce<sup>\*c</sup>

DOI: 10.1039/x0xx00000x

www.rsc.org/

**An neutral dinuclear Ir(III) Schiff base complex PIBIP has been synthesized and shown to exhibit both piezochromic luminescence (PCL) and aggregation induced emission (AIE) behaviour. An efficient second-level anti-counterfeit trademark and a data encryption device were fabricated using PIBIP as the active material.**

Anti-counterfeit and data security are important issues in economic and military fields as well as in our everyday lives.<sup>1</sup> This has led to the development of technologies such as infrared up-conversion,<sup>2</sup> magnetic response<sup>3</sup> and plasmonic security labels.<sup>4</sup> However, these systems are presently facing various problems such as poor stability and high reaction temperature (the calcination temperatures usually reach 800 °C).<sup>5</sup> Therefore, there is an urgent requirement for new advanced materials with high thermal stability and facile preparation to combat counterfeiting and information leakage.

Phosphorescent transition–metal complexes, such as Ir(III) systems, have a great potential in this area due to their high luminescence quantum yields, easy handling, structural versatility and high photostability.<sup>6</sup> However, traditional phosphorescent materials are usually regarded as first-level data encryption, with the disadvantage of security information being exposed immediately under ultraviolet (UV) light illumination. This means that encoded data is not secure and can be easily substituted by compounds with a similar emission colour. Therefore, the design of novel luminescent materials with more covert and reliable anti-counterfeit features is an appealing challenge. Piezochromic luminescent (PCL) compounds are a class of “smart” materials

whose fluorescent properties change in response to external pressure or mechanical grinding.<sup>7</sup> It has been shown that this process can be reversed and the original emission colour can be restored by altering the molecular packing mode in the solid state in response to external stimuli, such as heating or recrystallization.<sup>8</sup> Taking advantage of this reversible property, PCL materials are widely used in sensors, memory chips, and security inks.<sup>9</sup>

However, PCL compounds generally require sophisticated synthesis (>10 steps) to introduce different components into one molecule.<sup>10</sup> Moreover, similar to most conventional dyes, these luminophores suffer from aggregation caused quenching (ACQ), which results in low phosphorescence quantum yields in the solid state.<sup>11</sup> All the aforementioned drawbacks significantly limit the real-world applications of PCL materials. In contrast, aggregation-induced emission (AIE), as coined by Tang *et al.* in 2001,<sup>12</sup> is a property of compounds which emit weakly when dispersed in dilute solution but show strong emission when aggregated due to restricted intramolecular motions. This abnormal phenomenon has attracted considerable interest in the field of electroluminescent devices and chemical sensing.<sup>13</sup> The motivation for the present work is to develop phosphorescent transition–metal complexes with combined AIE and PCL properties and to exploit them as candidates for applications in anti-counterfeit and data encryption.

Herein, we designed and synthesized a new dinuclear Ir(III) complex (ppy)<sub>2</sub>Ir-(bsbd)-Ir(ppy)<sub>2</sub> (**PIBIP**) with a Schiff base bridging ligand (bsbdH<sub>2</sub>) and phenylpyridine (ppy) cyclometalating ligands (Scheme S1, ESI†). The photophysical properties demonstrate that **PIBIP** is AIE active and simultaneously shows PCL properties. Moreover, the emission colour of **PIBIP** can be converted to the original colour upon simple treatment by organic solvent. These results lead to the demonstration of a second-level anti-counterfeit trademark and data encryption device using **PIBIP** as security ink. **PIBIP** is the first neutral dinuclear Ir(III) complex which exhibits both PCL and AIE characteristics, to the best of our knowledge. These combined properties are important for device applications.<sup>7</sup> The flexible nature of the bsbd spacer allows the ligand to adopt optimal coordination geometries at the metal centres so as to facilitate the coexistence of PCL and AIE.

<sup>a</sup> Key Laboratory of Nanobiosensing and Nanobioanalysis at Universities of Jilin Province, Department of Chemistry, Northeast Normal University, 5268 Renmin Street, Changchun, Jilin Province 130024, P.R. China. E-mail: zhudx047@nenu.edu.cn; zmsu@nenu.edu.cn

<sup>b</sup> Key Laboratory of supramolecular structure and materials, Institute of Theoretical Chemistry, Jilin University, Changchun 130012, P. R. China.

<sup>c</sup> Department of Chemistry, Durham University, Durham, DH1 3LE, UK. E-mail: m.r.bryce@durham.ac.uk

† Electronic Supplementary Information (ESI) available: Experimental details, <sup>1</sup>H NMR spectra, absorption and emission spectra, crystallographic data. CCDC 1527325. See DOI: 10.1039/x0xx00000x

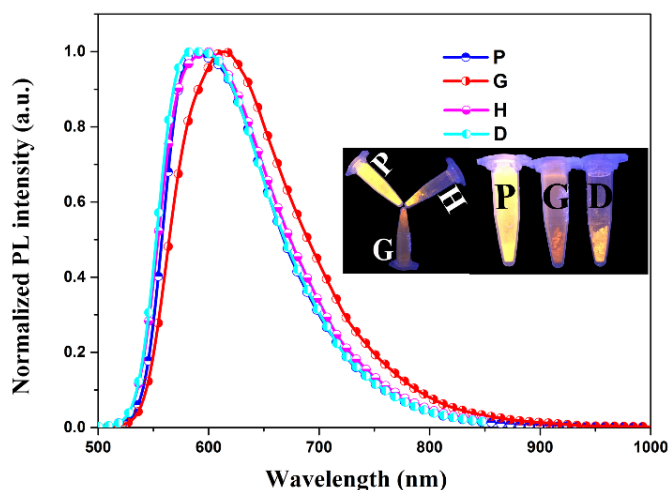


**Fig. 1** Emission spectra of unground "as synthesized" sample (**P**), ground sample (**G**), heated ground sample (**H**) and ground sample wetted with DCM (**D**). Inset: emission image of **P**, **G**, **H** and **D** under 365 nm UV illumination.

The structure of **PIBIP** was established by its  $^1\text{H}$  NMR and mass spectra, and single-crystal X-ray structure (ESI $^\dagger$ ). The pristine solid sample of **PIBIP** (hereafter abbreviated as **P**) shows yellow phosphorescence ( $\lambda_{\text{max}}=587$  nm), as shown in Fig. 1. When the powder **P** was thoroughly ground in an agate mortar for 5 min, a significant bathochromic shift ( $\lambda_{\text{max}}=613$  nm) was observed in the orange-emitting ground sample **G** (Fig. 1). The emission intensity of **G** shows a significant weakening that is clearly visible to naked eyes. The photoluminescence quantum yield (PLQY) is decreased dramatically in the grinding process from 20% (**P**) to 7% (**G**) (Table S1, ESI $^\dagger$ ). To investigate the reversibility of this PCL behavior, **G** was wetted with dropwise addition of dichloromethane (DCM) solvent (sample **D**) and the emission colour reverted to the initial emission colour of **P** within a few seconds (Fig. 1). Notably, the emission can perfectly revert to **G** when **D** was further ground. This PCL behaviour of **PIBIP** was shown to be highly reversible for several grinding-wetting cycles (Fig. S4, ESI $^\dagger$ ).

In order to establish the origin and mechanism of this reversible piezochromic behaviour of **PIBIP**, the  $^1\text{H}$  NMR spectra of both **P** and **G** were obtained. The results show

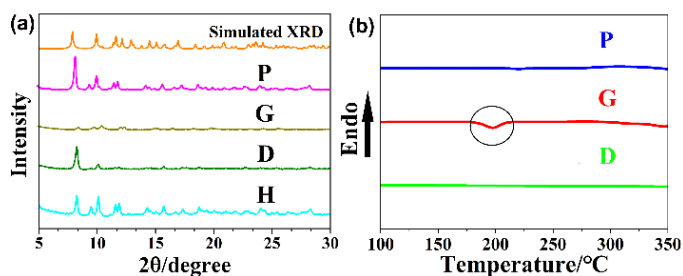


**Fig. 2** Powder X-ray diffraction patterns (a) and the DSC traces (b) of the corresponding samples.

complete consistency of chemical shift values and peak shapes for both **P** and **G** (Fig. S1, ESI $^\dagger$ ). The changed phosphorescent colours in the grinding process are, therefore, attributed to physical processes.

Powder X-ray diffraction (PXRD) was carried out to investigate the aggregation states of **P** and **G**. The sharp peaks in the XRD pattern (Fig. 2a) unambiguously show that the **P** sample is a well-ordered crystalline structure. In sharp contrast, the ground sample **G** exhibits weak and broad diffraction signals, which imply a crystalline to amorphous phase transition during the grinding process. The clear reflection peaks of pristine solid **P** reappeared after the sample **G** was heated (sample **H**) or wetted with dropwise DCM solvent (sample **D**). In addition, upon heating **G** to 350  $^\circ\text{C}$ , the DSC traces exhibited a clear broad exothermic recrystallization peak at *ca.* 198  $^\circ\text{C}$ . This peak is at a similar temperature at which thermal recrystallization begins to take place (Fig. 2b). Therefore, when **G** was heated at 198  $^\circ\text{C}$  for 1 min, the crystalline state was recovered and consequently the emission colour reverted to the original one (Fig. 1). **PIBIP** emitted only weakly in amorphous **G**, but became strongly emissive in crystalline **P**. This is typical crystallization-induced emission enhancement (CIEE) behaviour.<sup>14</sup> These results provide a rational explanation for the variation in PL intensity.

The single crystal X-ray structure analysis of **PIBIP** demonstrates that no intermolecular interactions exist in the molecular packing (Fig. S8, ESI $^\dagger$ ). By contrast, obvious intramolecular  $\pi$ - $\pi$  interactions between the bridging phenyl ring and the adjacent phenyl rings of ppy are observed (Fig. 3). This structure might be easily modified when mechanical pressure is applied, resulting in a red-shift of the PL spectra.<sup>15</sup> The excited-state lifetimes ( $\tau$ ) for **PIBIP** significantly decreased from **P** (0.97  $\mu\text{s}$ ) to **G** (0.49  $\mu\text{s}$ ) (Table S1, ESI $^\dagger$ ). Thus, it can be concluded that the changed  $\tau$  in the PCL process is associated with altering the solid-state molecular packing and/or the intramolecular interactions. The similar  $\tau$  of both the **P** and **D** states is consistent with them having the same molecular arrangement.<sup>16</sup>

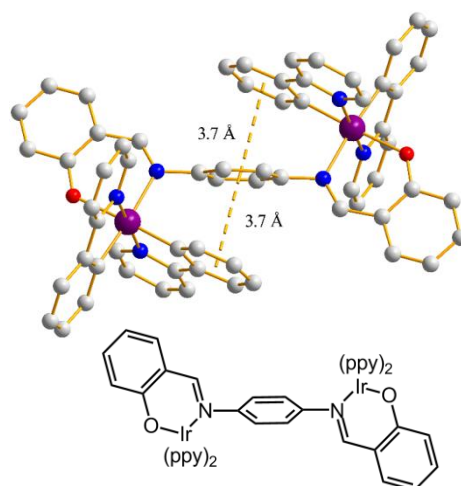


**Fig. 3** The X-ray molecular structure of **PIBIP** showing intramolecular  $\pi$ - $\pi$  interactions (dashed lines). Colour code: Ir purple; N blue; O red.

## COMMUNICATION

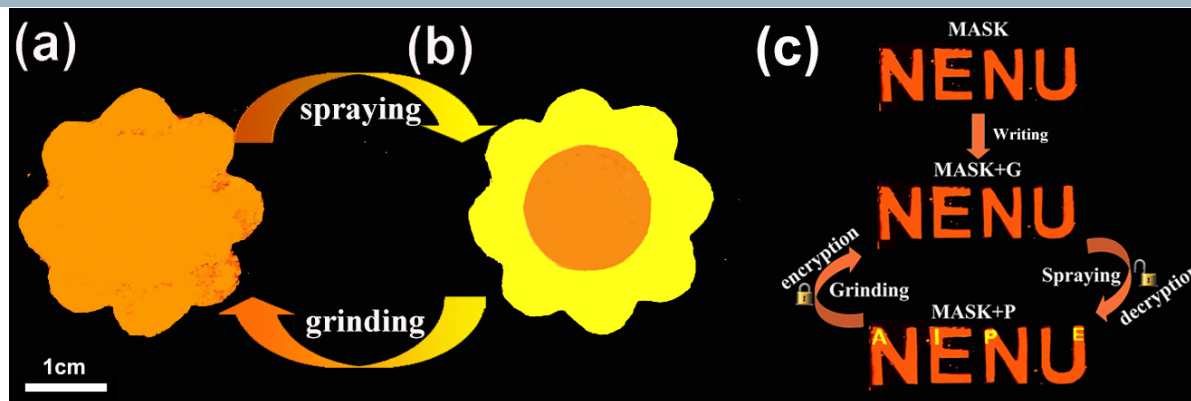


**Fig. 4** Photographic images of (a) first-level anti-counterfeit trademark (b) second-level anti-counterfeit trademark and (c) information encryption and decryption device. Note the appearance of the yellow letters 'AIPE' within the bottom 'NENU'.

Encouraged by the excellent PCL performance of **PIBIP**, anti-counterfeit trademark and data encryption devices were constructed (Fig. 4). **MASK** is a fluorescent emitter selected from the literature,<sup>17</sup> (for the structure see Fig. S2 in the ESI<sup>†</sup>) which shows a similar emission peak to **G** at around 610 nm (Fig. S3, ESI<sup>†</sup>). Thus, it is difficult to distinguish **G** from **MASK** due to their very similar emission colour and emission intensity. Furthermore, no colour change is observed when mechanical grinding is applied to **MASK**, which is an exclusive method to differentiate **G** and **MASK** (Fig. S3, ESI<sup>†</sup>). As shown in Fig. 4a and b, the anti-counterfeit trademark adopted the shape of a 'flower' comprising a central 'stamen' and a 'petal'. The 'stamen' is the as-prepared powder of **MASK** which emits orange fluorescence upon excitation with a 365 nm UV lamp and the 'petal' is the sample of **G** (detailed method is given in supporting information). This device could provide a second-level anti-counterfeit function. As shown in Fig. 4a, orange light was rapidly observed under the illumination of a standard UV lamp (at 254 and 365 nm), presenting a first-level anti-counterfeit system. When this 'flower' was sprayed with dichloromethane (DCM) solvent, the emission of the 'petal' changed immediately from orange (**G**) to yellow (**D**) (Fig. 4b). A second-level anti-counterfeit system was then successfully obtained as follows. Upon further grinding the 'petal', the original emission colour was regenerated and the first-level anti-counterfeit trademark reappeared (Fig. S5, ESI<sup>†</sup>).

Furthermore, a simple, convenient and efficient technology for data encryption and decryption was designed (Fig. 4c). **G** was used as a 'cryptographic ink' while **MASK** was used as a control reagent. In the encryption stage, the characters 'NENU' were written on a filter paper by using **MASK**, then the powder **G** was carefully spread on it as the letters 'AIPE'. So **G** was hidden by **MASK** even under UV light, because **G** and **MASK** emitted unitary orange light. In the decryption stage, the yellow security letters 'AIPE' appeared clearly

when DCM solvent was sprayed onto the as-prepared letters 'NENU'. In contrast to the orange-emitting background, the letters 'AIPE' showed intense yellow emission which is in agreement with the change in emission colour from **G** to **D**. Moreover, 'AIPE' can be easily hidden again by grinding. This simple process demonstrates an excellent encryption and decryption reversibility for several cycles. These data suggest that complex **PIBIP** has the potential to be employed in practical applications as an anti-counterfeit and security protection ink with simple optical authentication.

Since **PIBIP** exhibits strong luminescence in the solid state (Table S2, ESI<sup>†</sup>), the AIE property was probed by using different ratios of THF-water mixtures. As shown in Fig. 5, **PIBIP** exhibits very

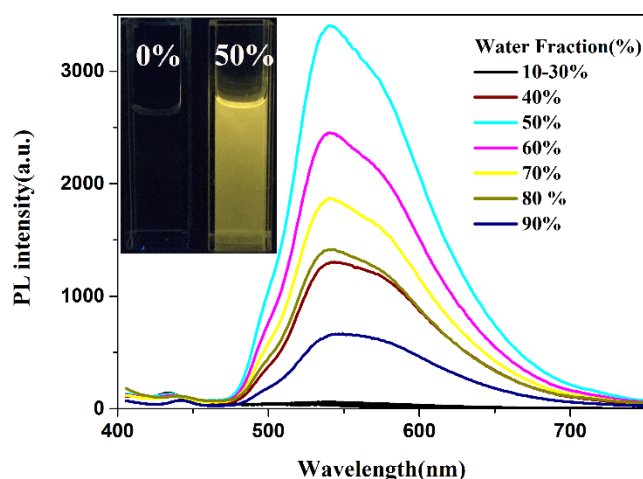


**Fig. 5** Emission spectra of **PIBIP** in THF-water mixtures with different water fractions (0-90% v/v) at room temperature. Inset: emission image of **PIBIP** in pure THF solution and THF-water mixture (50% water fraction) under 365 nm UV illumination.

weak emission in pure THF solution, where it was well dissolved. Nevertheless, the PL intensity was dramatically enhanced when the water fraction reached 50%, increasing by a maximum of up to about 100-fold in comparison with pure THF solution. The PL intensity then decreased with increasing water content >50% water fraction, but the PL intensity at 90% water fraction is still stronger than in pure THF solution. There are two possible reasons for this behaviour. First, after aggregation, the molecules covered within the surface of the nanoparticles did not emit light, leading to a decrease in phosphorescent intensity. Second, crystalline particles and amorphous particles simultaneously form when the water fraction is increased. The former particles would enhance emission intensity but the latter do not.<sup>8</sup> Thus, the measured overall PL intensity depends on the combined actions of the two kinds of nanoparticles. Furthermore, the UV-visible absorption profile showed a Mie scattering effect for the mixtures of **PIBIP** with high water content (Fig. S6, ESI<sup>†</sup>).<sup>18</sup> Transmission electron microscopy (TEM) and electron diffraction (ED) experiments indicated that amorphous molecular aggregates are formed in the mixtures (Fig. S7, ESI<sup>†</sup>).<sup>19</sup> Evidently, **PIBIP** is an excellent AIE chromophore that could effectively suppress non-radiative decay to produce intense emission in the solid state.

In summary, a smart dinuclear Ir(III) Schiff base complex **PIBIP** shows simultaneous reversible PCL behaviour and AIE-activity. An obvious bathochromic shift occurs in the solid state upon mechanical grinding, and this new emission reverts to the original state after wetting with DCM solvent. Anti-counterfeiting trademark and data encryption devices have been successfully constructed by combining **PIBIP** and fluorescent **MASK** through the piezochromic and solvatochromic properties of **PIBIP**. Therefore, these findings indicate that **PIBIP** could expand the applications of PCL materials to anti-counterfeiting, information storage and data security protection.

The work was funded by NSFC (No.51473028), the key scientific and technological project of Jilin province (20150204011GX, 20160307016GX), the development and reform commission of Jilin province (20160058). Work in Durham was funded by EPSRC grant EP/K039423/1.

## Notes and references

- (a) M. You, M. Lin, S. Wang, X. Wang, G. Zhang, Y. Hong, Y. Dong, G. Jin and F. Xu, *Nanoscale*, 2016, **8**, 10096-10104; (b) M. You, J. Zhong, Y. Hong, Z. Duan, M. Lin and F. Xu, *Nanoscale*, 2015, **7**, 4423-4431; (c) T. Zhang, L. Fu, Z. Chen, Y. Cui and X. Liu, *Progress in Organic Coatings*, 2016, **100**, 100-104; (d) P. Kumar, S. Singh and B. K. Gupta, *Nanoscale*, 2016, **8**, 14297-14340.
- J. F. Suyver, A. Aebischer, D. Biner, P. Gerner, J. Grimm, S. Heer, K. W. Krämer, C. Reinhard and H. U. Güdel, *Optical Mater.*, 2005, **27**, 1111-1130.
- R. Li, Y. Zhang, J. Tan, J. Wan, J. Guo and C. Wang, *Appl. Mater. Interfaces*, 2016, **8**, 9384-9394.
- Y. Cui, R. S. Hegde, I. Y. Phang, H. K. Lee and X. Y. Ling, *Nanoscale*, 2014, **6**, 282-288.
- J. M. Meruga, W. M. Cross, P. Stanley May, Q. Luu, G. A. Crawford and J. J. Kellar, *Nanotechnology*, 2012, **23**, 395201.
- (a) H. Sun, S. Liu, W. Lin, K. Y. Zhang, W. Lv, X. Huang, F. Huo, H. Yang, G. Jenkins, Q. Zhao and W. Huang, *Nat. Commun.*, 2014, **5**, 3601; (b) H. Sasabe, J. Takamatsu, T. Motoyama, S. Watanabe, G. Wagenblast, N. Langer, O. Molt, E. Fuchs, C. Lennartz and J. Kido, *Adv. Mater.*, 2010, **22**, 5003-5007; (c) M. Mydlak, C. Bizzarri, D. Hartmann, W. Sarfert, G. Schmid and L. De Cola, *Adv. Funct. Mater.*, 2010, **20**, 1812-1820.
- Z. Chi, X. Zhang, B. Xu, X. Zhou, C. Ma, Y. Zhang, S. Liu and J. Xu, *Chem. Soc. Rev.*, 2012, **41**, 3878-3896.
- (a) M. Luo, X. Zhou, Z. Chi, S. Liu, Y. Zhang and J. Xu, *Dyes and Pigments*, 2014, **101**, 74-84; (b) Q. Lu, X. Li, J. Li, Z. Yang, B. Xu, Z. Chi, J. Xu and Y. Zhang, *J. Mater. Chem. C*, 2015, **3**, 1225-1234; (c) X. Zhang, Z. Ma, Y. Yang, X. Zhang, Z. Chi, S. Liu, J. Xu, X. Jia and Y. Wei, *Tetrahedron*, 2014, **70**, 924-929.
- (a) A. Pucci, F. Di Cuia, F. Signori and G. Ruggeri, *J. Mater. Chem.*, 2007, **17**, 783-790; (b) Y. Dong, J. W. Y. Lam, A. Qin, J. Liu, Z. Li, B. Z. Tang, J. Sun and H. S. Kwok, *Appl. Phys. Lett.*, 2007, **91**, 011111; (c) Z. Ning, Z. Chen, Q. Zhang, Y. Yan, S. Qian, Y. Cao and H. Tian, *Adv. Funct. Mater.*, 2007, **17**, 3799-3807; (d) S. Hirata and T. Watanabe, *Adv. Mater.*, 2006, **18**, 2725-2729; (e) A. Kishimura, T. Yamashita, K. Yamaguchi and T. Aida, *Nat. Mater.*, 2005, **4**, 546-549.
- C. Ma, B. Xu, G. Xie, J. He, X. Zhou, B. Peng, L. Jiang, B. Xu, W. Tian, Z. Chi, S. Liu, Y. Zhang and J. Xu, *Chem. Commun.*, 2014, **50**, 7374-7377.
- Z. Zhang, Z. Wu, J. Sun, P. Xue and R. Lu, *RSC Adv.*, 2016, **6**, 43755-43766.
- J. Luo, Z. Xie, J. W. Y. Lam, L. Cheng, B. Z. Tang, H. Chen, C. Qiu, H. S. Kwok, X. Zhan, Y. Liu and D. Zhu, *Chem. Commun.*, 2001, 1740-1741.
- J. Mei, N. L. Leung, R. T. Kwok, J. W. Lam and B. Z. Tang, *Chem. Rev.*, 2015, **115**, 11718-11940.
- J. Tong, Y. J. Wang, Z. Wang, J. Z. Sun and B. Z. Tang, *J. Phys. Chem. C*, 2015, **119**, 21875-21881.
- (a) Y. Dong, B. Xu, Y. J. Zhang, X. Tian, L. Wang, J. Chen, H. Lv, S. Wen, B. Li, L. Ye, B. Zou and W. Tian, *Angew. Chem. Int. Ed.*, 2012, **51**, 10782-10785; (b) Q. Qi, J. Qian, X. Tan, L. Wang, B. Xu, B. Zou and W. Tian, *Adv. Funct. Mater.*, 2015, **25**, 4005-4010.
- Y. Han, H. T. Cao, H. Z. Sun, Y. Wu, G. G. Shan, Z. M. Su, X. G. Hou and Y. Liao, *J. Mater. Chem. C*, 2014, **2**, 7648-7655.
- R. K. Shah, K. S. Abou-Melha, F. A. Saad, T. Yousef, G. A. A. Al-Hazmi, M. G. Elghalban, A. M. Khedr and N. El-Metwaly, *J. Therm. Anal. Calorim.*, 2015, **123**, 731-743.
- B. Xu, W. Li, J. He, S. Wu, Q. Zhu, Z. Yang, Y.-C. Wu, Y. Zhang, C. Jin, P.-Y. Lu, Z. Chi, S. Liu, J. Xu and M. R. Bryce, *Chem. Sci.*, 2016, **7**, 5307-5312.
- G. G. Shan, H. B. Li, J. S. Qin, D. X. Zhu, Y. Liao and Z. M. Su, *Dalton Trans.*, 2012, **41**, 9590-9593.

---

## Supporting Information

### A neutral dinuclear Ir(III) complex for anti-counterfeiting and data encryption.

Yang Jiang,<sup>a</sup> Guangfu Li,<sup>a</sup> Weilong Che,<sup>a</sup> Yingjie Liu,<sup>b</sup> Bin Xu,<sup>b</sup> Guogang Shan,<sup>a</sup> Dongxia Zhu,<sup>\*a</sup> Zhongmin Su,<sup>\*a</sup> Martin R. Bryce<sup>\*c</sup>

---

<sup>a</sup> Key Laboratory of Nanobiosensing and Nanobioanalysis at Universities of Jilin Province, Department of Chemistry, Northeast Normal University, 5268 Renmin Street, Changchun, Jilin Province 130024, P.R. China. E-mail: [zhudx047@nenu.edu.cn](mailto:zhudx047@nenu.edu.cn); [zmsu@nenu.edu.cn](mailto:zmsu@nenu.edu.cn)

<sup>b</sup> Key laboratory of supramolecular structure and materials, Institute of Theoretical Chemistry, Jilin University, Changchun 130012, P. R. China.

<sup>c</sup> Department of Chemistry, Durham University, Durham, DH1 3LE, UK. E-mail: [m.r.bryce@durham.ac.uk](mailto:m.r.bryce@durham.ac.uk)

#### Contents:

1. Experimental - general information
2. <sup>1</sup>H NMR spectra of **PIBIP** and **MASK** at room temperature
3. Photophysical properties
4. X-ray crystallographic data
5. References

## 1. Experimental - general information

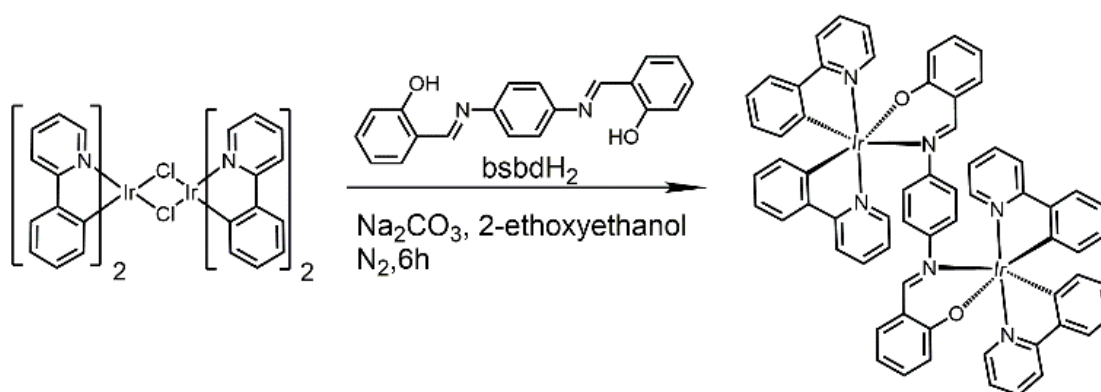
Materials obtained from commercial suppliers were used without further purification unless otherwise stated. All glassware, syringes, magnetic stirring bars, and needles were thoroughly dried in a convection oven. Reactions were monitored using thin layer chromatography (TLC). Commercial TLC plates were used and the spots were visualised under UV light at 254 and 365 nm.  $^1\text{H}$  NMR spectra were recorded at 25 °C on a Varian 500 MHz spectrometer. The chemical shifts ( $\delta$ ) are given in parts per million relative to internal standard TMS. The  $^1\text{H}$  NMR spectra were referenced internally to the residual proton resonance in  $\text{DMSO-}d_6$  ( $\delta$  2.49 ppm) or  $\text{CDCl}_3$  ( $\delta$  7.24 ppm). Powder X-ray diffraction (XRD) patterns of the samples were collected on a Rigaku Dmax 2000. Differential scanning calorimetry (DSC) curves were obtained with a NETZSCH thermal analysis DSC200 F<sub>3</sub> under argon with a heating rate 10 °C min<sup>-1</sup>. Transmission electron microscopy (TEM) and electron diffraction analyses of the samples were obtained using a TECNAI F20 microscope. The samples were prepared by placing microdrops of the solution on a holey carbon copper grid. UV-vis absorption spectra were recorded on a Shimadzu UV-3100 spectrophotometer. Photoluminescence spectra were collected on a Shimadzu RF-5301pc spectrophotometer and Maya 2000Pro optical fiber spectrophotometer. PL efficiencies were measured with an integrating sphere (C-701, Labsphere Inc.) with a 365 nm Ocean Optics LLS-LED as the excitation source, and the laser was introduced into the sphere through an optical fiber. The excited-state lifetimes were measured by exciting the samples with 385 nm light pulses with ~3 ns pulse width from a Quanta-Ray DCR-2 pulsed Nd: YAG laser. The X-ray crystal structure data of complex **PIBIP** were collected on a Bruker Smart Apex II CCD diffractometer with graphite-monochromated Mo K $\alpha$  radiation ( $\lambda = 0.71069 \text{ \AA}$ ) at room temperature.

### PIBIP synthesis and characterisation

#### Synthesis of $(\text{ppy})_2\text{Ir}(\text{bsbd})\text{-Ir}(\text{ppy})_2$ (**PIBIP**) (Scheme S1)

A yellow suspension of the dichloro-bridged diiridium complex  $[\text{Ir}(\text{ppy})_2\text{Cl}]_2$ <sup>[1]</sup> (0.353 g, 0.33 mmol), bridging ligand  $\text{bsbdH}_2$ <sup>[2]</sup> (0.104 g, 0.33 mmol) and  $\text{Na}_2\text{CO}_3$  (0.349 g, 3.2 mmol) in 2-ethoxyethanol was stirred at 135 °C for 6 hours under a nitrogen atmosphere and the suspension was then filtered and the precipitate was washed with diethyl ether and

water. Then the crude product was dried and purified by silica gel column chromatography with dichloromethane/methyl alcohol (10:1 v/v) as eluent. **PIBIP** was obtained as a yellow crystalline solid in 76% yield (0.315 g).  $^1\text{H}$  NMR (500 MHz, DMSO- $d_6$ ,  $\delta$  [ppm]):  $\delta$  8.69 (d,  $J=5$  Hz, 1H); 8.56 (d,  $J=10$  Hz, 1H); 8.12 (d,  $J=10$  Hz, 1H); 7.90 (d,  $J=10$  Hz, 1H); 7.86 (d,  $J=10$  Hz, 2H); 7.79 (s, 1H); 7.68 (d,  $J=10$  Hz, 1H); 7.32 (t,  $J=10$  Hz, 2H); 7.27 (t,  $J=10$  Hz, 1H); 7.23 (d,  $J=5$  Hz, 2H); 7.17 (t,  $J=5$  Hz, 1H); 6.77 (t,  $J=10$  Hz, 1H); 6.59 (t,  $J=5$  Hz, 1H); 6.53 (t,  $J=10$  Hz, 1H); 6.41 (d,  $J=10$  Hz, 1H); 6.37 (t,  $J=5$  Hz, 1H); 6.32 (t,  $J=10$  Hz, 1H); 5.98 (d,  $J=5$  Hz, 1H); 5.77 (d,  $J=10$  Hz, 1H); 5.37 (t,  $J=5$  Hz, 1H). MS: (MALDI-TOF) [m/z]: 1315.48 (calcd: 1316.29). Anal. Calcd. for  $\text{C}_{64}\text{H}_{46}\text{Ir}_2\text{N}_6\text{O}_2$ : C 58.43, H 3.52, N 6.39. Found C 58.56, H 3.50, N 6.41. Single crystals for X-ray analysis were grown by diffusion of acetone into a solution of **PIBIP** in dimethyl sulfoxide.



**Scheme S1** Synthetic route to complex **PIBIP**.

### Trademark manufacturing method

The anti-counterfeit trademark adopted the shape of a ‘flower’ comprising a central ‘stamen’ and a ‘petal’. Two specific moulds (filter paper with holes) are made for regulating the shape of as-prepared powder **MASK** and **G**. The ‘stamen’ is **MASK** and it was spread on a filter paper with a central round hole. Then remove this filter paper and substitute another one which hole is in the shape of petal. **G** is carefully spread within the hole and remove this filter paper so that the whole ‘flower’ can be demonstrated.

Procedure for conversion of **D** to **G**. **D** was ground completely by a porcelain pestle on a filter paper. It is easily hand-held because the moderate grinding strength with the pestle is easily realized by human force. The excitation illuminating sources of the anti-counterfeit trademark are always using from UV light (254 or 365nm).

## 2. $^1\text{H}$ NMR Spectra of PIBIP and MASK at room temperature

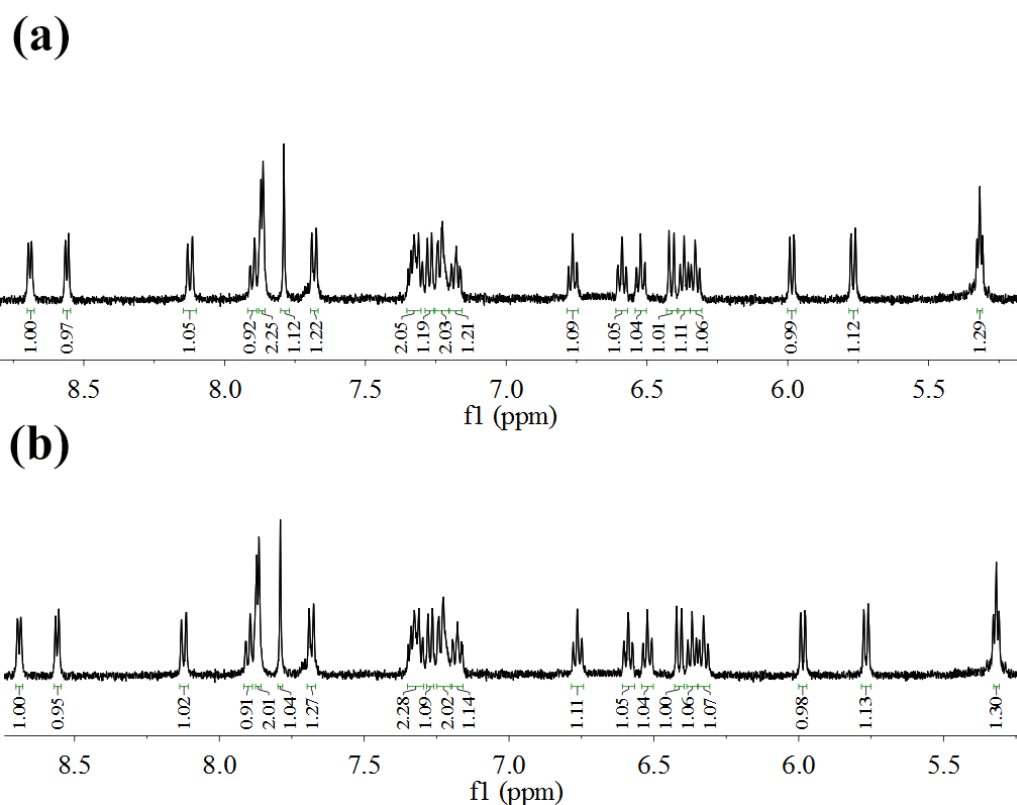


**Fig. S1**  $^1\text{H}$  NMR spectra of **PIBIP** in  $\text{DMSO-d}_6$  before grinding (a) and after grinding (b).



**Fig. S2**  $^1\text{H}$  NMR spectrum of **MASK** in  $\text{CDCl}_3$  at room temperature.

### 3. Photophysical properties

**Table S1** The phosphorescent emission efficiency ( $\Phi_{em}$ ) and excited-state lifetimes ( $\tau$ ) in various states of **PIBIP**.

	As-synthesized ( <b>P</b> )	Ground ( <b>G</b> )	CH <sub>2</sub> Cl <sub>2</sub> wetted ( <b>D</b> )	Heated ( <b>H</b> )
$\Phi_{em}$	0.20	0.07	0.26	0.19
$\tau$ ( $\mu$ s)	0.97	0.49	0.85	0.64

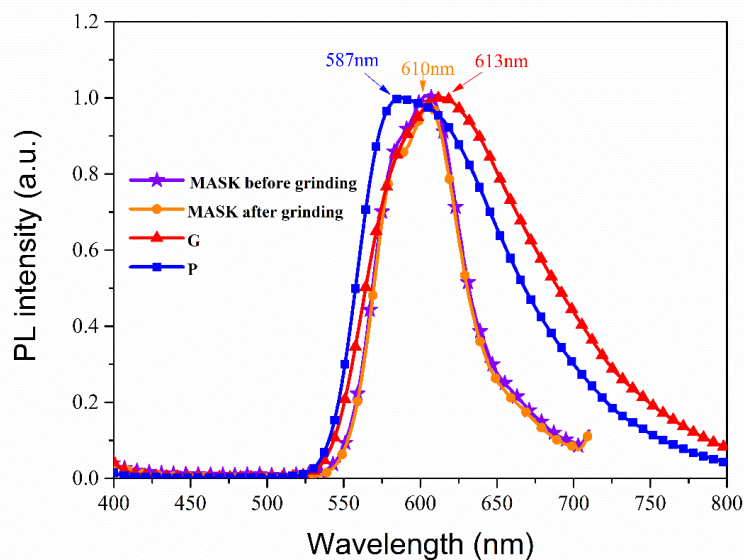


**Fig. S3** The emission spectra of unground sample **MASK** and ground sample **MASK** compared with comparable states **P** and **G** of **PIBIP**.

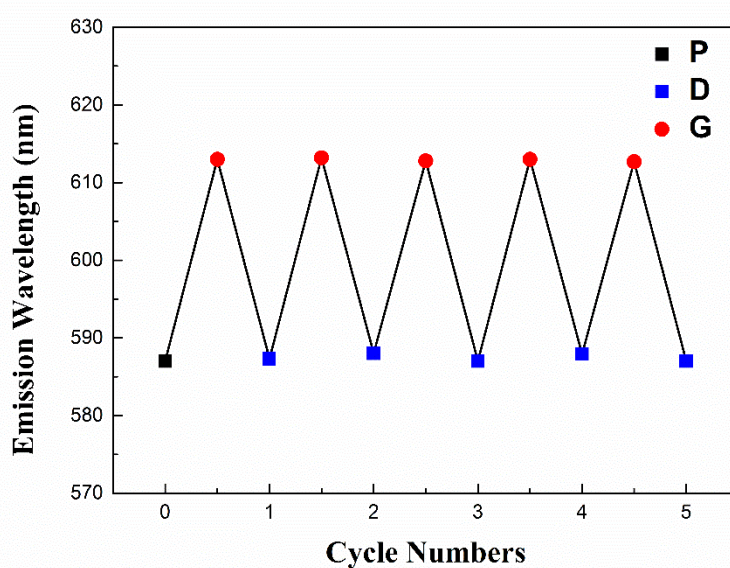


**Fig. S4** Maximum emission wavelength of **PIBIP** through five cycles of states **D** and **G**.

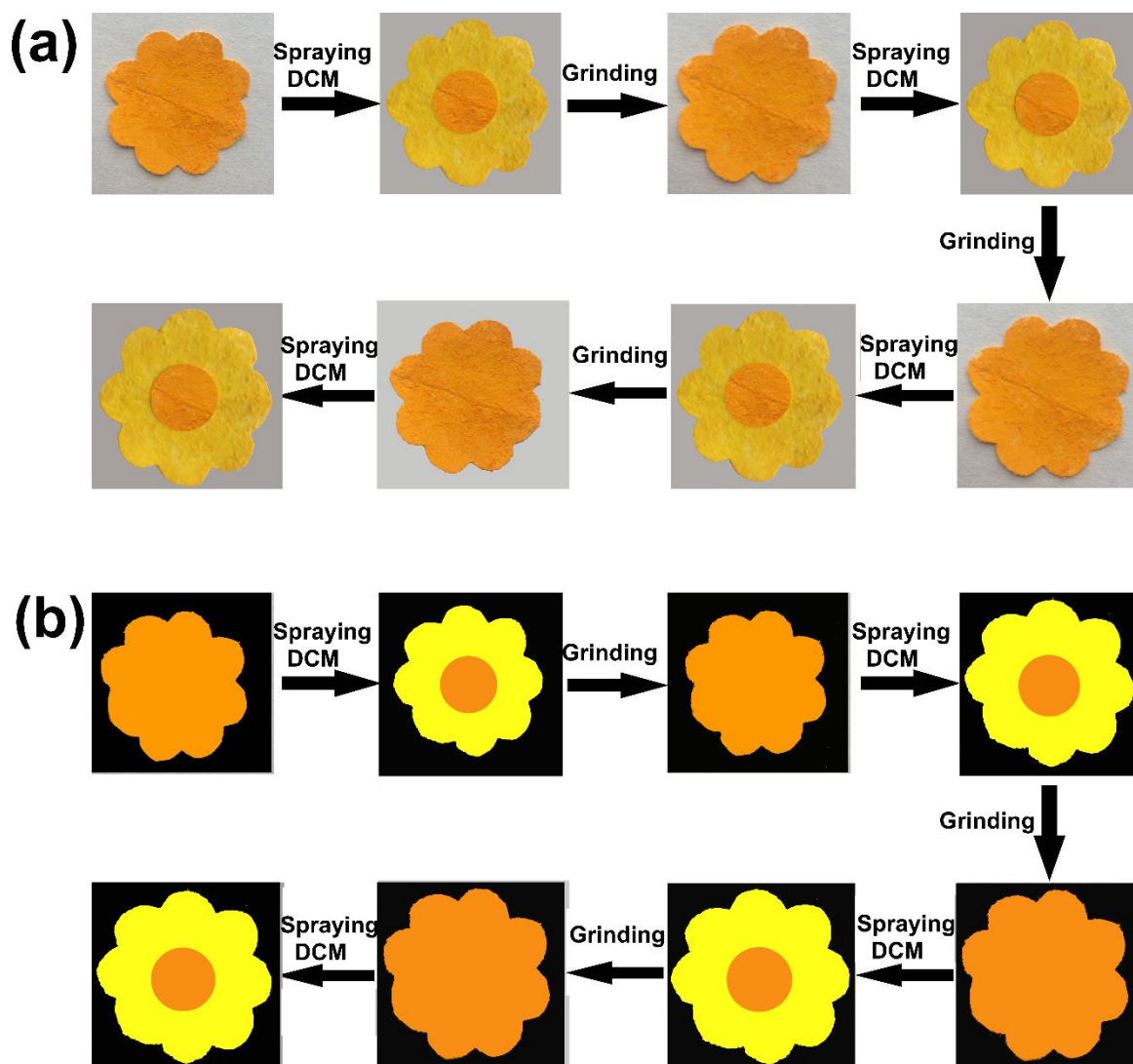


**Fig. S5** Photographic images of anti-counterfeit trademark with several reversible spraying and grinding processes under (a) daylight and (b) UV light

**Table S2** Photophysical characteristics of **PIBIP**.

Absorption and emission at room temperature			Emission at 77 K		
$\lambda_{\text{abs}}^{\text{a}}$ (nm)	$\lambda_{\text{em}}^{\text{b}}$ (nm)	$\Phi_{\text{em}}^{\text{b}}(\tau^{\text{b}}[\mu\text{s}])$	$\lambda_{\text{em}}^{\text{c}}$ (nm)	$K_{\text{r}} \times 10^6 \text{ s}^{-1}$	$K_{\text{nr}} \times 10^6 \text{ s}^{-1}$
208(0.629),	587	0.20(0.99)	584	0.20	0.80
252(0.321)					

<sup>a</sup>Measured in THF ( $1.0 \times 10^{-5}$  M). <sup>b</sup>Measured in solid state ( $\lambda_{\text{exc}}=385$  nm; error for  $\Phi_{\text{L}} \pm 5\%$ ).  
<sup>c</sup>In THF glass.

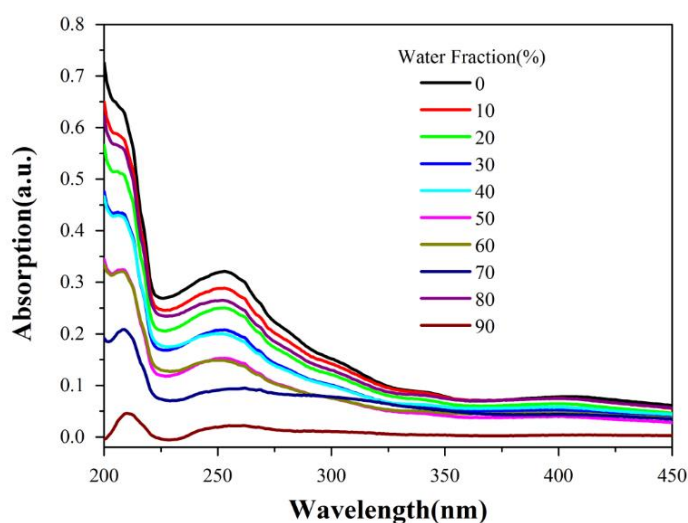


**Fig. S6** UV-visible absorption spectra of **PIBIP** in acetonitrile-water mixtures with different water fractions (0-90%, v/v) at room temperature.

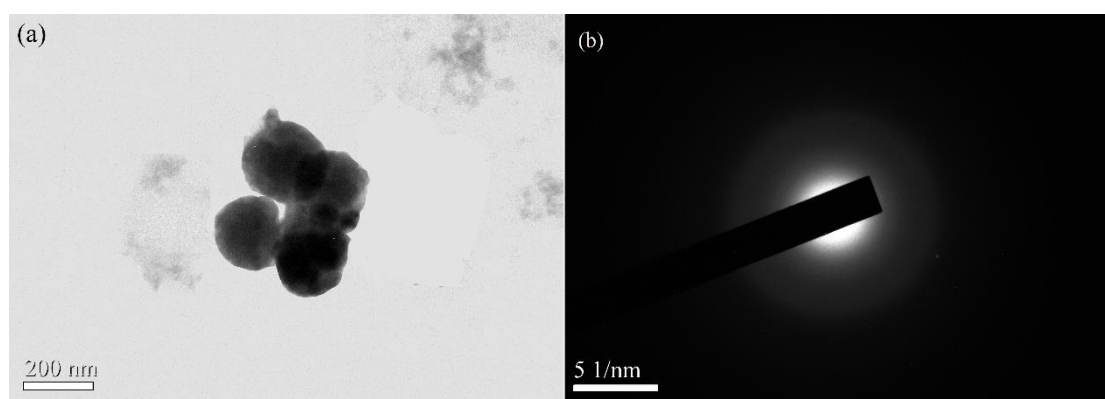


**Fig. S7** (a) TEM image of nanoaggregates of **PIBIP** formed in THF-H<sub>2</sub>O mixtures with 50% water fraction. (b) Electron diffraction pattern of the amorphous nanoaggregates.

#### 4. X-ray crystallographic data

The molecular structure of **PIBIP** was confirmed by X-ray crystallographic analysis of single crystals. Diffraction data were collected on a Bruker SMART Apex CCD diffractometer using  $k(\text{Mo-K}\alpha)$  radiation ( $k = 0.71069 \text{ \AA}$ ). Cell refinement and data reduction were made by the SAINT program. The structure was determined using the SHELXTL/PC program. The crystallographic data have been deposited with the Cambridge Crystallographic Data Centre with CCDC deposition number 1527325. These data can be obtained free of charge from The Cambridge Crystallographic Data Centre via [www.ccdc.cam.ac.uk/data\\_request/cif](http://www.ccdc.cam.ac.uk/data_request/cif).

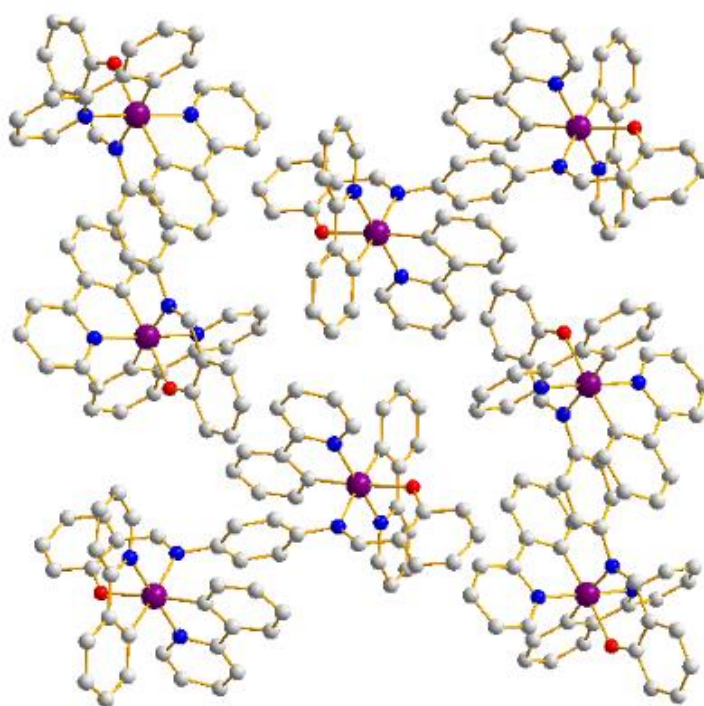


**Fig. S8** Molecular packing of **PIBIP** in the crystal. Color code: Ir purple; N blue; O red.

**Table S3** Crystal data and structure refinement for **PIBIP**.

	<b>PIBIP</b>
Empirical formula	C <sub>64</sub> H <sub>46</sub> Ir <sub>2</sub> N <sub>6</sub> O <sub>2</sub>
Formula weight	1316.29
Temperature (K)	293(2)
Crystal system	Monoclinic
Space group	P2(1)/c
a/Å	11.434(5)
b/Å	14.581(5)
c/Å	18.230(5)
α/°	90.000(5)
β/°	101.210(5)
γ/°	90.000(5)
V/Å <sup>3</sup>	2981.3(18)
Z	4
P <sub>calc</sub> (g/cm <sup>3</sup> )	1.880
μ/mm <sup>-1</sup>	6.751
R <sub>int</sub>	0.0636
Goodness-of-fit on F <sup>2</sup>	1.414
R <sub>1</sub> <sup>a</sup> , wR <sub>2</sub> <sup>b</sup> [I > 2σ(I)]	0.0503, 0.1464
R <sub>1</sub> , wR <sub>2</sub> (all data)	0.0775, 0.1699

$$^a R_1 = \frac{\sum ||F_o| - |F_c||}{\sum |F_o|}, \quad ^b wR_2 = \left\{ \frac{\sum [w(F_o^2 - F_c^2)^2]}{\sum [w(F_o^2)^2]} \right\}^{1/2}$$

## 5. References

1. K. A. King, P. J. Spellane and R. J. Watts, *J. Amer. Chem. Soc.*, 1985, **107**, 1431-1432.
2. C. Yao, C. Niu, N. Na, D. He and J. Ouyang, *Anal. Chim. Acta*, 2015, **853**, 375-383.